

Article

Numerical Study of Scale Effects on Open Water Propeller Performance

Carlo Giorgio Grlj , Nastia Degiuli * , Andrea Farkas  and Ivana Martić

Faculty of Mechanical Engineering and Naval Architecture, University of Zagreb, Ivana Lučića 5,
10000 Zagreb, Croatia

* Correspondence: nastia.degiuli@fsb.hr

Abstract: The present study aims to investigate the scale effects of the open water propeller performance using computational fluid dynamics (CFD). The results are presented for the propeller which was previously 3D scanned and digitized. The results obtained using two turbulence models within the numerical simulations are compared. The verification study is conducted to assess the numerical uncertainty and thus obtain the optimal grid size for the numerical simulations. A transition model is used at the model scale to account for the partially laminar flow. The propeller is then scaled, and numerical simulations are performed to assess the scale effects on the open water performance of the considered propeller. The results demonstrate the significant scale effects on open water characteristics however, scale effects are considerably lower when the transition model is applied within the numerical simulations at the model scale.

Keywords: CFD; open water test; scale effect; propeller; transition model; turbulence model



Citation: Grlj, C.G.; Degiuli, N.; Farkas, A.; Martić, I. Numerical Study of Scale Effects on Open Water Propeller Performance. *J. Mar. Sci. Eng.* **2022**, *10*, 1132. <https://doi.org/10.3390/jmse10081132>

Academic Editors: Jasna Prpic-Orsic and Luca Braidotti

Received: 21 July 2022

Accepted: 16 August 2022

Published: 17 August 2022

Publisher's Note: MDPI stays neutral with regard to jurisdictional claims in published maps and institutional affiliations.



Copyright: © 2022 by the authors. Licensee MDPI, Basel, Switzerland. This article is an open access article distributed under the terms and conditions of the Creative Commons Attribution (CC BY) license (<https://creativecommons.org/licenses/by/4.0/>).

1. Introduction

The open water test (OWT) is carried out in towing tanks to assess the hydrodynamic performance of propellers. These tests are always performed at a model scale since open water tests at full-scale would be expensive and there are no testing sites where such large-scale tests would be feasible. Nowadays, computational fluid dynamics (CFD) is successfully used by many researchers for the assessment of ship propulsion performance. Farkas et al. [1] used numerical simulations for the prediction of the nominal wake in the case of a bulk carrier. The authors noticed significant scale effects in both integral values of nominal wake and circumferential averaged non-dimensional axial velocity distribution. Jang et al. [2] employed numerical simulations of OWT at model scale to assess the influence of pitch motion on the propeller performance. The authors demonstrated that the pitch motion of the ship has a dominant effect on the variation of the propeller performance resulting in the sinusoidal pitch motion of the propeller. Sun et al. [3] used CFD to investigate the vibration and noise reduction effects of an energy-saving device. The obtained results showed that the considered energy-saving device can improve propulsion efficiency and reduce the radiation noise intensity. Multiple different scaling methods have been developed for the extrapolation of the model scale to full-scale results. Helma et al. [4] presented an overview of the different scaling methods and assessed their influence on the full-scale results. The authors divided the scaling methods into statistical, analytical, CFD methods, and a combination of the listed methods. Helma [5] developed a scaling procedure for unconventional propeller designs called the β_i method utilizing the equivalent profile concept. The author showed that the method works well with all propeller geometries since it is independent of the blade loading distribution. It is also important to point out that it needs the results from only one set of open water curves. Extrapolation performed by any of the scaling methods provides accurate and reliable results [6], but experimental OWT is cost-intensive and time-consuming. CFD is a reasonable alternative to towing tank

tests since it is a versatile tool that can be used to predict ship hydrodynamic characteristics in model and full-scale [7]. The authors showed in [7] that the numerical results of the ship resistance in calm water varied from -10% to 4% compared to sea trials data. Mikkelsen and Walther [8] validated the results from the self-propulsion numerical simulations against the results obtained from the sea trials. They showed that the discrepancy between the results can be further lowered using the modified wall functions for the simulation of the surface roughness. The difference between the obtained delivered powers is largely affected by propellers operating at higher Reynolds numbers in full-scale simulations [9]. Another problem with extrapolation to full-scale is the fact that the scaling methods are not accurate enough for unconventional propellers [10]. Multiple authors addressed this issue by simulating the flow around the full-scale propellers with unconventional geometries such as tip-modified propellers [5,11,12]. The hydrodynamic analysis of a tip-loaded propeller was performed using the boundary element method to evaluate the propeller-induced hull pressures in [13]. The predicted hull pressures are in good agreement with the ones obtained in the cavitation tunnel and with unsteady RANS equations at the design and moderately loaded conditions. Dong et al. [12] studied the influence of PPTC-II propeller's tip rake on the scale effects by conducting numerical simulations in full-scale and model scale as well as modifying the propeller geometry with and without the tip rake. The authors compared the results with the ones obtained using the ITTC-1978 method and concluded that the ITTC method must be updated to predict the scale effects on the thrust and torque coefficients more precisely. Li et al. The study by [10] also concluded that ITTC should develop new scaling methods for unconventional propellers. Chen et al. [14] studied the open water hydrodynamic performance of a high skew submarine propeller E1619 and concluded that the difference between the predicted torque coefficient using the ITTC 1978 method and the ones obtained by numerical simulations is not negligible. Furthermore, they concluded that the law of scale effect cannot be analyzed using only two models and that several different scales must be considered. Owen et al. [15] investigated the effect of biofouling on the propeller open water performance using numerical simulations at the model scale where multiple methods for propeller rotation modeling were used, i.e., the moving reference frame (MRF) method and sliding mesh (SM) approach. Minor discrepancies between the open water results obtained from the two methods were shown; thus, the authors decided to retain the MRF method since it is computationally less expensive. The same method was used in [16,17] since it lowers the computational time, and the convergence is faster than using the overset mesh (OM) method. Mikkelsen et al. [18] also used the MRF method for open water simulations; however, in the case of self-propulsion simulations, the MRF method was used only to initialize the flow around the propeller followed by the SM method for the rest of the simulation. A comparison of SM and OM methods was given in [19] for the case of a rotating vertical axis turbine. The authors showed that by increasing the number of cells the results converge faster using the OM method at the cost of 10% higher computational time. Wang et al. [20] used a single-run procedure and OM method to determine the open water curves. The results were compared to the experimental results performed by IIHR (available at the Tokyo 2015 CFD Workshop [21]) and an overall agreement between the results was shown. Bekhit and Lungu [22] performed numerical simulations of resistance and self-propulsion tests with and without the rudder as well as OWT. The obtained results were compared with experimental results, showing an average error of about 3% for the thrust coefficient and 7% for the torque coefficient. Lungu [23] in his later study performed numerical simulations of the resistance, open water, and self-propulsion tests of a 3600 TEU containership, where he showed a 5% difference between the measurements and numerical predictions of thrust and torque coefficients. Farkas et al. [24] compared two methods for assessing the influence of biofouling on the open water propeller characteristics. The verification and validation study were performed for three full-scale propellers and satisfactory agreement was achieved. These results were compared with the results obtained using a propeller performance prediction method for fouled surfaces. The impact of hard fouling on the ship hydrodynamic performance was assessed in [25], where

the authors conducted full-scale CFD simulations of OWT for three propellers and validated the results using the towing tank results. Farkas et al. [26] investigated the effects of biofilm on ship propulsion characteristics. The authors demonstrated the significant impact of biofilm on the ship hydrodynamic performance highlighting the importance of keeping the hull clean. Dogrul [27] investigated the scale effects of a self-propelled submarine where he compared the extrapolated numerical results with the results from full-scale simulations. Gonzalez-Adalid et al. [28] conducted model scale and full-scale numerical simulations for the determination of the performance of two unconventional propellers with the transition model. Good agreement was shown between the results obtained from the fully turbulent, full-scale simulations and the sea trial data. Baltazar et al. [29] also performed the numerical simulations with the transition model at the model scale, but in addition, the paint test results were used for the validation study. The authors showed an increase in thrust of 2–4% when using the transition model. Moran-Guerrero et al. [30] used an improved Gamma Reynolds Theta ($\gamma - Re_\theta$) correlation-based model for transition prediction, which considers the crossflow effects. Pawar and Brizzolara [31] used the same transition model to simulate the OWT of an open and ducted propeller to assess the discrepancies between experimental and numerical results.

The focus of this study is the investigation of the scale effects of the open water propeller performance. The numerical simulations are conducted for multiple scales ranging from model scale to full-scale. First, the verification study is conducted using the grid convergence index (GCI) method, and the results of the numerical simulations are presented. The rest of the paper is organized as follows: the numerical model and the grid generation are described within Methods section. The results are presented and briefly discussed in the Results section and discussion followed by the conclusions from the present study in the last section.

2. Methods

2.1. Numerical Modeling

The numerical simulations in this study are based on the Reynolds-averaged Navier–Stokes (RANS) equations. For the case of an incompressible fluid, continuity and momentum transport equations for unsteady flow are written as:

$$\frac{\partial \bar{u}_i}{\partial x_i} = 0 \tag{1}$$

$$\rho \frac{\partial \bar{u}_i}{\partial t} + \rho \frac{\partial}{\partial x_j} (\bar{u}_i \bar{u}_j + \overline{u'_i u'_j}) = -\frac{\partial \bar{p}}{\partial x_i} + \frac{\bar{\tau}_{ij}}{\partial x_j} \tag{2}$$

where \bar{u}_i is the averaged Cartesian components of the velocity vector, $\overline{\rho u'_i u'_j}$ is the Reynolds stress tensor (RST), \bar{p} is the mean pressure, and $\bar{\tau}_{ij}$ is the mean viscous stress tensor defined as:

$$\bar{\tau}_{ij} = \mu \left(\frac{\partial \bar{u}_i}{\partial x_j} + \frac{\partial \bar{u}_j}{\partial x_i} \right) \tag{3}$$

where μ is the dynamic viscosity of the fluid.

To discretize the governing equations, the finite volume method (FVM) is used in the simulations. Within the numerical simulations, the shear stress transport $k - \omega$ (SSTKO) turbulence model is used to close the system of discretized differential equations since it is accurate enough in the near wall and far-field region [32]. The SSTKO is compared with the realizable $k - \epsilon$ (RKE) turbulence model.

The rotation of the propeller can be modeled using three approaches, i.e., SM, OM, and steady-state simulation using the MRF. In this study, the MRF method [33] is used since it is computationally more efficient compared to the other two approaches [15]. The MRF is a steady-state method that consists of a rotating flow around a stationary mesh.

2.2. Turbulence Models

RANS turbulence models are based on the modeling of RST which is expressed as a function of the mean flow quantities. The turbulence models applied in this study use the concept of turbulent eddy viscosity μ_t to model RST.

2.2.1. Realizable $k - \epsilon$ (RKE) Turbulence Model

This is a two-equation model that solves transport equations for the turbulent kinetic energy k and the turbulent dissipation rate ϵ . The eddy viscosity in this model is described with the following equation:

$$\mu_t = \rho C_\mu \frac{k^2}{\epsilon} \tag{4}$$

where C_μ is the model coefficient.

The transport equations for k and ϵ within the RKE model are defined as:

$$\frac{\partial}{\partial t}(\rho k) + \frac{\partial}{\partial x_i}(\rho k \bar{u}_i) = \frac{\partial^2 k}{\partial x_i^2} \left(\mu + \frac{\mu_t}{\sigma_k} \right) + f_c G_k + G_b - \Upsilon_M - \rho(\epsilon - \epsilon_0) + S_k \tag{5}$$

$$\frac{\partial}{\partial t}(\rho \epsilon) + \frac{\partial}{\partial x_i}(\rho \epsilon \bar{u}_i) = \frac{\partial^2 \epsilon}{\partial x_i^2} \left(\mu + \frac{\mu_t}{\sigma_\epsilon} \right) + \frac{1}{T_e} C_{\epsilon 1} (f_c S k + C_{\epsilon 3} G_b) - C_{\epsilon 2} f_2 \rho \left(\frac{\epsilon}{T_e} - \frac{\epsilon_0}{T_0} \right) + S_\epsilon \tag{6}$$

where \bar{u}_i is the averaged velocity vector, f_c is the curvature correction factor, G_k is the turbulent production term, σ_k and σ_ϵ are turbulent Schmidt numbers, G_b is the buoyancy production term, ϵ_0 is the ambient turbulence value that counteracts turbulence decay, Υ is the dilatation dissipation, $C_{\epsilon 1}$, $C_{\epsilon 2}$ and $C_{\epsilon 3}$ are the model depending coefficients, S is the modulus of the mean strain tensor, and finally S_k and S_ϵ are the user-defined source terms.

2.2.2. Shear Stress Transport $k - \omega$ (SSTKO) Turbulence Model

The modified standard $k - \omega$ model blends $k - \epsilon$ model in the far field with the $k - \omega$ model near the walls. Turbulent eddy viscosity in this model is given by the following equation:

$$\mu_t = \rho k T \tag{7}$$

where T is the turbulent time scale.

The $k - \omega$ turbulence model solves two transport equations for the turbulent kinetic energy k and the specific dissipation ω :

$$\frac{\partial}{\partial t}(\rho k) + \frac{\partial}{\partial x_i}(\rho k \bar{u}_i) = \frac{\partial^2 k}{\partial x_i^2} (\mu + \sigma_k \mu_t) + G_k + G_{nl} + G_b - \rho \beta^* f_{\beta^*} (\omega k - \omega_0 k_0) + S_k \tag{8}$$

$$\frac{\partial}{\partial t}(\rho \omega) + \frac{\partial}{\partial x_i}(\rho \omega \bar{u}_i) = \frac{\partial^2 \omega}{\partial x_i^2} (\mu + \sigma_\omega \mu_t) + G_\omega + D_\omega - \rho \beta f_\beta (\omega^2 - \omega_0^2) + S_\omega \tag{9}$$

where σ_k , σ_ω , β , β^* are the model depending coefficients, G_{nl} is the non-linear production term, f_{β^*} is the free-shear modification factor, f_β is the vortex-stretching modification factor, and finally k_0 and ω_0 are the ambient values that counteract turbulence decay.

2.3. Transition Model

The turbulence model assumes that the flow is turbulent in the whole flow region. Within the numerical simulations at the model scale, the flow is expected to be partly laminar. To model the transition from laminar to turbulent flow, a transition model should be applied. The correlation-based $\gamma - Re_\theta$ transition model is used within the numerical simulations because it is coupled with the SSTKO turbulence model. The transition model

solves two additional transport equations, i.e., intermittency γ and transition momentum thickness Reynolds number $\overline{Re}_{\theta t}$ which read as follows:

$$\frac{\partial(\rho\gamma)}{\partial t} + \frac{\partial(\rho U_j \gamma)}{\partial x_j} = P_\gamma - E_\gamma + \frac{\partial}{\partial x_j} \left[\left(\mu + \frac{\mu_t}{\sigma_f} \right) \frac{\partial \gamma}{\partial x_j} \right] \tag{10}$$

$$\frac{\partial(\rho \overline{Re}_{\theta t})}{\partial t} + \frac{\partial(\rho U_j \overline{Re}_{\theta t})}{\partial x_j} = P_{\theta t} + \frac{\partial}{\partial x_j} \left[\sigma_{\theta t} (\mu + \mu_t) \frac{\partial \overline{Re}_{\theta t}}{\partial x_j} \right] \tag{11}$$

where U_j is the mean velocity vector, P_γ and $P_{\theta t}$ are the production terms, E_γ is the destruction term, σ_f and $\sigma_{\theta t}$ are the model coefficients. More information on the production, destruction terms and model coefficients can be found in [34]. To accurately solve the laminar and transitional boundary layers, the first cell near the wall must have $y^+ \leq 1$ [29]. Because of this constraint, it is decided to disable the transition model at other scales.

2.4. Open Water Propeller Characteristics

The open water characteristics of a propeller consist of determining the forces and moments acting on the propeller which is operating in a uniform stream without the influence of the hull. To obtain the open water curves, thrust K_T and torque K_Q coefficients need to be determined as functions of the advance coefficient J . The thrust and torque coefficients are defined using the following equations:

$$K_T = \frac{T}{\rho n^2 D^4} \tag{12}$$

$$K_Q = \frac{Q}{\rho n^2 D^5} \tag{13}$$

where T and Q are the thrust and torque, respectively, ρ is the fluid density, n the propeller rate of revolution, and D the propeller diameter. The advance coefficient is defined as follows:

$$J = \frac{v_A}{nD} \tag{14}$$

where v_A is the speed of advance.

Finally, propeller open water efficiency η_o is defined by:

$$\eta_o = \frac{J K_T}{2\pi K_Q} \tag{15}$$

2.5. Grid Generation

The computational domain is defined as a cylinder that encloses the propeller with the hub and shaft. The domain boundaries are placed sufficiently far from the propeller to avoid their influence on the obtained results. Figure 1 shows the computational domain with the respective dimensions.

For the discretization of the computational domain, the unstructured hexahedral mesh is used. The numerical simulations with the transition model are performed with a grid that has $y^+ \leq 1$, while the remaining simulations are performed with a grid that has $y^+ > 30$ [35]. To obtain the required y^+ values, the distance from the wall to the center of the first prism layer is determined using the following equation:

$$y = \frac{y^+ \nu}{u_\tau} \tag{16}$$

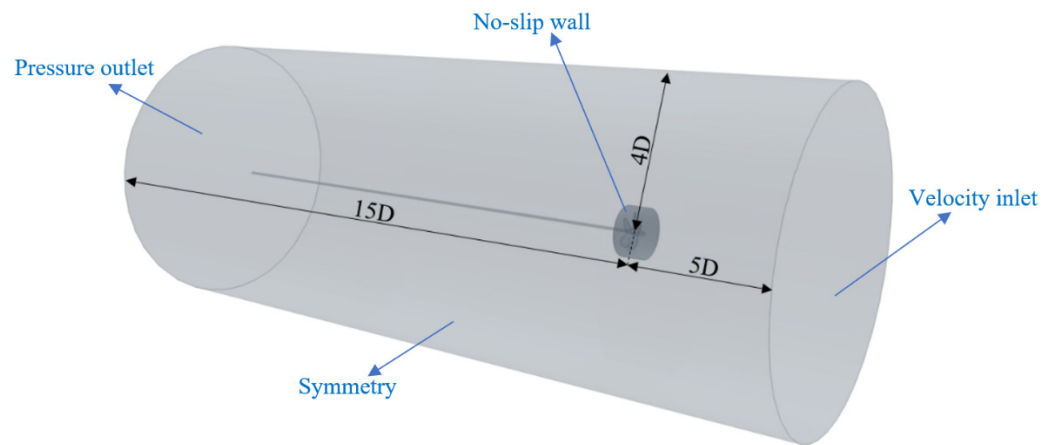


Figure 1. Computational domain for OWT.

The frictional velocity u_τ is calculated as follows:

$$u_\tau = \sqrt{\frac{\tau_w}{\rho}} \tag{17}$$

where the wall shear stress τ_w is calculated using the skin friction coefficient C_f :

$$\tau_w = \frac{1}{2} C_f \rho U_\infty^2 \tag{18}$$

In this study, the skin friction coefficient is determined for a flat plate using the following equation:

$$C_f = 0.0576 Re_d^{-1/5} \tag{19}$$

where Reynolds number depends on the scale. While this is not an exact method for the determination of the height of the first prism layer, it yields satisfactory results. The obtained y^+ values are checked, and it is ensured that $y^+ > 30$ in numerical simulations where wall functions are applied and that $y^+ < 1$ in numerical simulations with the transition model. Special attention is given to the refinement around the propeller and in the MRF zone. The transition from the prism layer to the core mesh is carefully discretized to avoid possible numerical diffusion. A more detailed discussion regarding the influence of y^+ values on the obtained numerical results regarding the open water test can be found in Owen et al. [15].

2.6. Verification Study

The GCI method, based on the Richardson extrapolation is used for the verification study. The GCI method is used to determine the appropriate grid size by determining the grid uncertainty. If the iterative uncertainty is neglected, then the numerical uncertainty consists only of the grid uncertainty. The interested reader can find more details about the method in [24].

2.7. Case Study

In this study, a propeller is modeled using computer-aided design (CAD) software. The modeled propeller has geometric properties that resemble the one used for the Japan CFD Workshop 2015 for the Japan Bulk Carrier (JBC). The propeller is then scaled and the numerical simulations of OWT are conducted. Figure 2 shows the 3D scan of the propeller model and the CAD model used in the numerical simulations. Table 1 contains the propeller main particulars, and the scales used in the CFD simulations are listed within the same table. The advance coefficients are obtained by changing the speed of advance

with a constant rate of revolution of the propeller. The rate of revolution for different scales is defined using the following equation:

$$n_s = \frac{n_m}{\sqrt{\lambda}} \tag{20}$$

where n_s is the rate of revolution at the specific scale and n_m is the rate of revolution at the model scale.

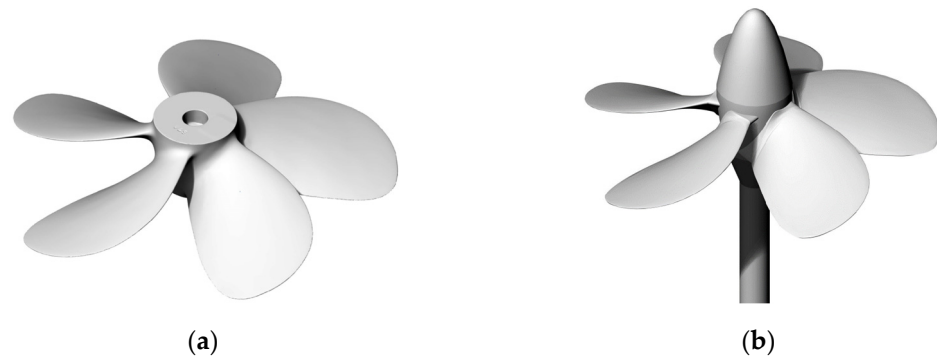


Figure 2. The geometry of the stock propeller. Three-dimensional scan (a), CAD model (b).

Table 1. The main particulars of the considered propeller in the different scales.

Scale, λ	40.264	4	2	1.333	1
Index	M	M1	M2	M3	F
Diameter, D (m)	0.203	2.040	4.079	6.119	8.158
Rate of revolution, n (rps)	26.03	8.204	5.801	4.737	4.102
Reynolds number, (Re) (-)	1.298×10^6	4.111×10^7	1.162×10^8	2.136×10^8	3.309×10^8
Pitch ratio, (P/D) (-)			0.736		
Expanded area ratio, A_e/A_0 (-)			0.644		
Hub ratio, d/D (-)			0.193		
Number of blades, Z (-)			5		

3. Results and Discussion

3.1. Verification Study

Firstly, the verification study is performed using the numerical simulations at the model scale with the transition model. Since the numerical simulations are steady state, only the GCI for the spatial discretization is calculated. Table 2 shows the data of the used grids where the grid spacing h is calculated using the following equation:

$$h = \sqrt[3]{\frac{1}{N} \sum_{i=1}^N (\Delta V_i)} \tag{21}$$

where N is the total number of finite volume cells and V_i is the volume of the i -th cell. The grid refinement ratio is calculated as follows:

$$r_{ij} = \frac{h_i}{h_j} \tag{22}$$

The GCI is calculated for the open water efficiency η_o in the range of advance coefficient from 0.1 to 0.6. Table 3 presents the obtained GCIs with the calculated averages as well. Both the average coarse and fine GCIs are low, and the coarse GCI is under 4 %; thus, the medium grid size is used for the rest of the numerical simulations.

Table 2. Number of cells, grid spacing, and grid refinement ratio for model scale numerical simulations with the transition model.

Index	Number of Finite Volume Cells, N	Grid Spacing, h (m)	Grid Refinement Ratio, r
1	8.8M	0.0098	1.164
2	5.2M	0.0114	
3	3.0M	0.0119	1.040

Table 3. Fine and coarse GCI for the range of advance coefficients and their average for model scale.

J	GCI_{fine} , %	GCI_{coarse} , %
0.1	1.258	1.71
0.2	1.878	3.14
0.3	5.239	15.25
0.4	0.116	2.21
0.5	0.002	0.55
0.6	0.017	0.65
Average	1.42	3.92

Another verification study is conducted for three full-scale grids with non-dimensional wall distance $y^+ > 30$. The coarse and fine GCI are calculated for open water efficiency in the considered range of advance coefficients. Table 4 presents the details about the grids, while Table 5 shows the calculated grid convergence indices for the open water efficiency.

Table 4. Number of cells, grid spacing, and grid refinement ratio for full-scale numerical simulations.

Index	Number of Finite Volume Cells, N	Grid Spacing, h (m)	Grid Refinement Ratio, r
1	10.2M	0.3758	1.090
2	8M	0.4075	
3	4.5M	0.0119	1.207

Table 5. Fine and coarse GCI for the range of advance coefficients and their average for full-scale.

J	GCI_{fine} , %	GCI_{coarse} , %
0.1	0.42	0.19
0.2	1.70	1.34
0.3	7.65	8.06
0.4	1.82	2.19
0.5	1.48	1.90
0.6	1.55	2.15
Average	2.44	2.64

This study shows that the average GCI in the range of advance coefficient from 0.1 to 0.6 are less than 4% and the difference between the coarse and fine GCI is negligible. Thus, a medium grid size can be used for the full-scale simulations. The grids for the other scales use the same grid setup with varying prism layers to maintain $y^+ > 30$, so it is expected that the GCI will not differ significantly from the two studies presented.

3.2. Turbulence Models

The influence of the turbulence model on the obtained results is investigated using the model scale and full-scale numerical simulations with the medium grid size and the non-dimensional wall distance $y^+ > 30$. Figures 3 and 4 show the open water curves

obtained from the model and full-scale numerical simulations, respectively. The influence of the turbulence model on the results is barely visible for the full-scale case. The relative difference in the open water efficiency for the SSTKO turbulence model is equal to 2.83% for model scale and 0.65% for full-scale. The transition model is disabled for both cases shown in the figures.

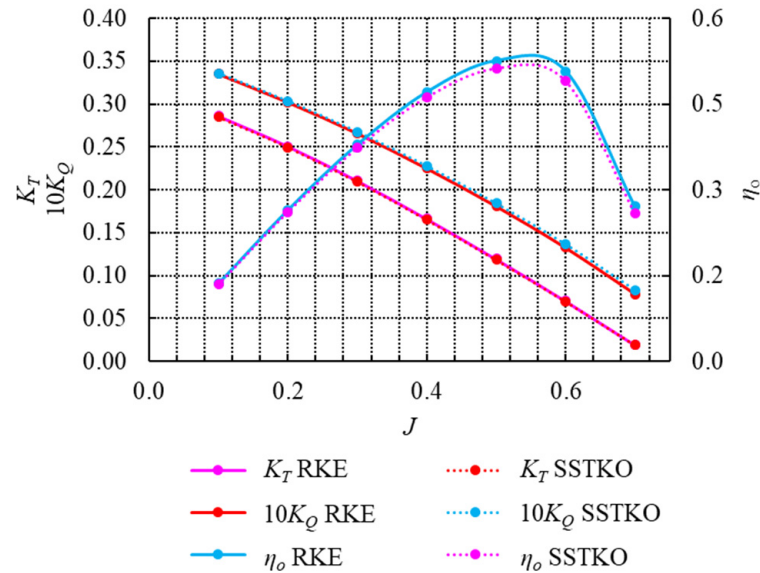


Figure 3. The open water curves of model scale propeller obtained using RKE and SSTKO turbulence models.

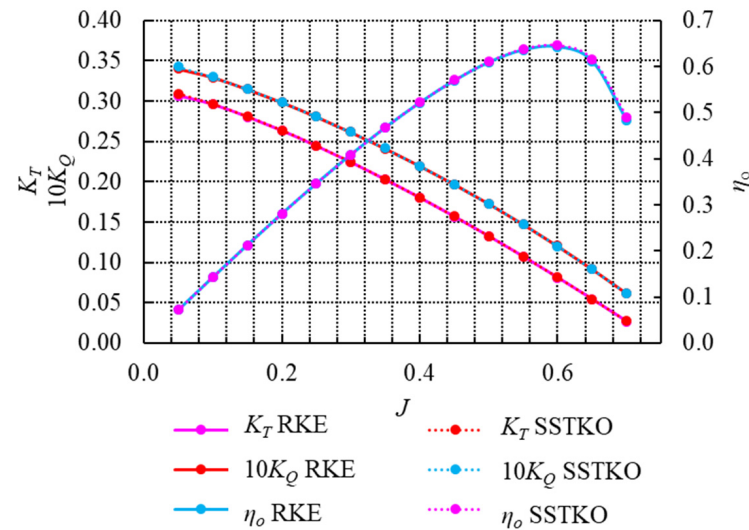


Figure 4. The open water curves of full-scale propeller obtained using RKE and SSTKO turbulence models.

3.3. Model Scale

The numerical simulations at the model scale are performed for non-dimensional wall distance $y^+ > 30$ and $y^+ \leq 1$. The open water curves for the first case are already presented in the previous subsection. Figure 5 shows the open water curves for the numerical simulations at the model scale with and without the transition model for the case with $y^+ \leq 1$. Table 6 shows the numerical values of the relative errors, with respect to the case with the transition model, at different advance coefficients and the average values as well.

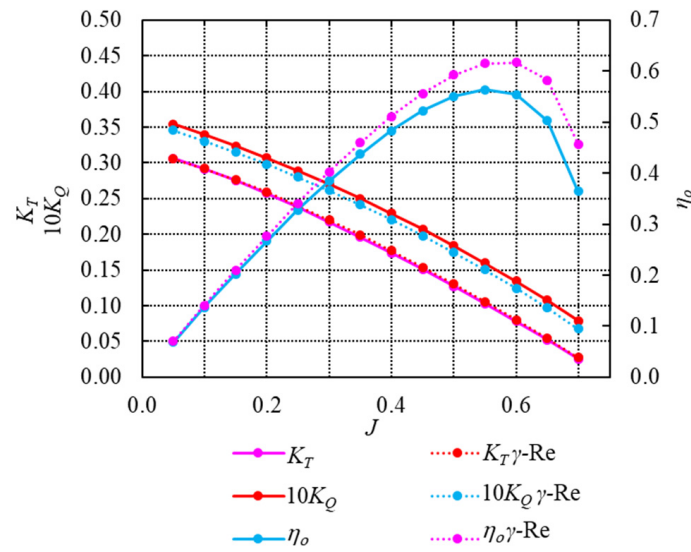


Figure 5. Open water curves for model scale with and without the transition model.

Table 6. Relative differences between the thrust and torque coefficients and open water efficiencies in the range of advance coefficients.

J	K_T , %	$10K_Q$, %	η_o , %
0.2	0.38	2.14	−1.72
0.4	−0.65	4.30	−4.74
0.6	−2.83	8.40	−10.36
0.7	−10.30	17.38	−23.58
Average	3.54	8.06	10.10

The data shows lower values of the torque coefficient for the case with the transition model enabled, which in turn leads to higher values of the open water efficiency. It can be seen that the transition model influences the torque coefficient more in comparison to the thrust coefficient.

Figures 6 and 7 show the distribution of the skin friction coefficient obtained from the model scale numerical simulations. Significant differences between the two cases can be noticed. The skin friction coefficient is lower in the case with the transition model, which is expected considering the partially laminar flow. The lower skin friction leads to lower values of the torque coefficient which results in higher open water efficiencies.

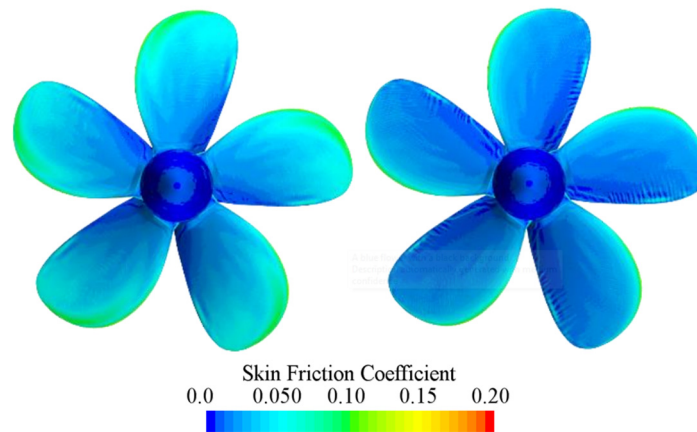


Figure 6. Distribution of the skin friction coefficient on the suction side obtained from numerical simulations at model scale for $J = 0.7$ without transition model (left) and with transition model (right).

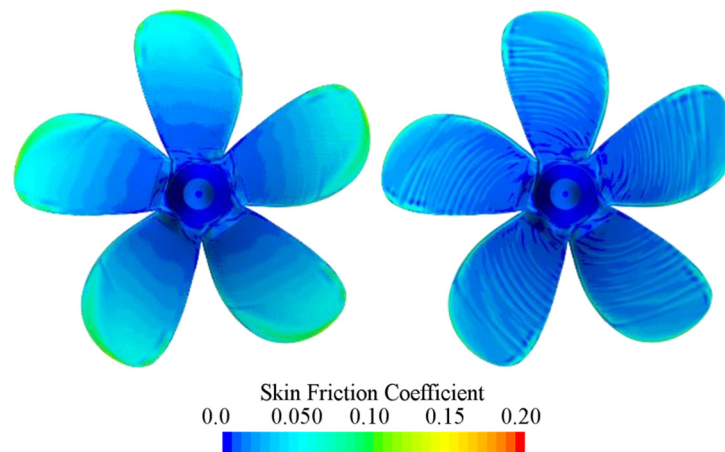


Figure 7. Distribution of the skin friction coefficient on the pressure side obtained from numerical simulations at model scale for $J = 0.7$ without transition model (**left**) and with transition model enabled (**right**).

3.4. Scale Effects

The open water curves obtained from numerical simulations at different scales are compared in this subsection. Figure 8 shows the open water efficiency as a function of the advance coefficient obtained from the simulations at different scales. Figures 9 and 10 show the thrust and torque coefficients, respectively. In Figures 8–10, the numerical results at the model scale are extrapolated to full-scale using the ITTC 1978 Performance Prediction Method (PPM). It can be noticed that the differences between the open water efficiencies are more apparent at higher advanced coefficients. The open water efficiency at the full-scale obtained using ITTC 1978 PPM is higher than at the model scale. However, the extrapolated values of open water efficiency are lower than the ones obtained using numerical simulations in full-scale. This can be attributed to the fact that ITTC 1978 PPM considers a rough full-scale propeller, while in this study smooth full-scale propeller is analyzed.

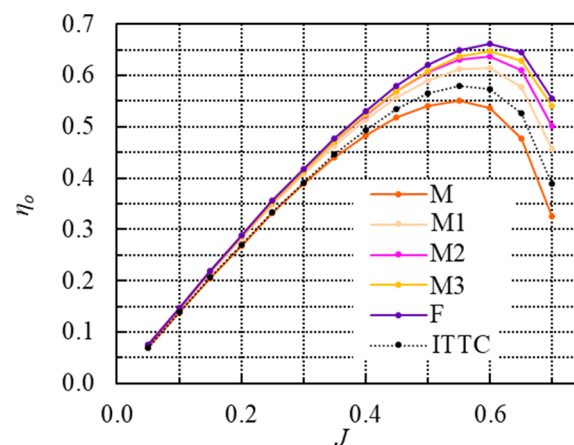


Figure 8. Open water efficiency as a function of advance coefficient for different scales.

Figure 8 shows that the open water efficiency increases with the decrease in scale. Minor discrepancies between the open water efficiencies are visible in the range of lower advance coefficients. The thrust coefficients decrease with the increase in scale, while the torque coefficients decrease with the decrease in scale. This tendency can be seen over the entire range of advance coefficients. It should be noted that the scale effects on the frictional component of the thrust and torque are significant, while the scale effects on the pressure component of the thrust and torque are relatively low [36]. Bhattacharyya et al. [36] noticed that the pressure component has a positive contribution, and the friction component has a negative contribution to the value of propeller thrust at any scale. On the other hand,

the absolute contributions from the pressure and friction components to the total torque are positive at any scale. At higher Re numbers, the portion of frictional components in the total torque and thrust values are lower in comparison to the portion of the frictional components in the total torque and thrust values at lower Re numbers, since the scale effects of the frictional component of the thrust and torque are significant. Since the frictional component has a positive contribution to the total torque, the torque coefficients will be lower at higher Re numbers. On the other hand, since the frictional component has a negative contribution to the total thrust, the thrust coefficients will be higher at higher Re numbers.

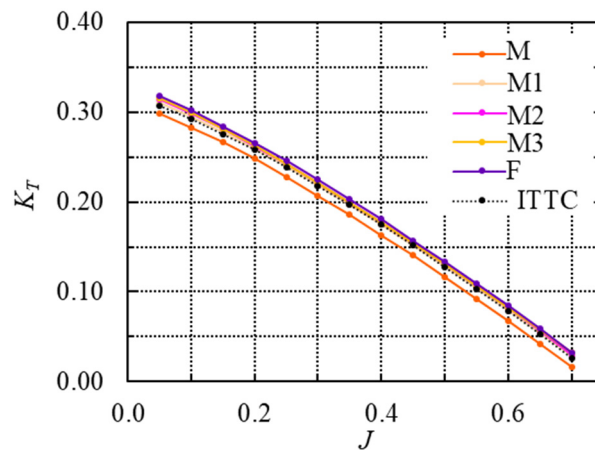


Figure 9. Thrust coefficient as a function of advance coefficient for different scales.

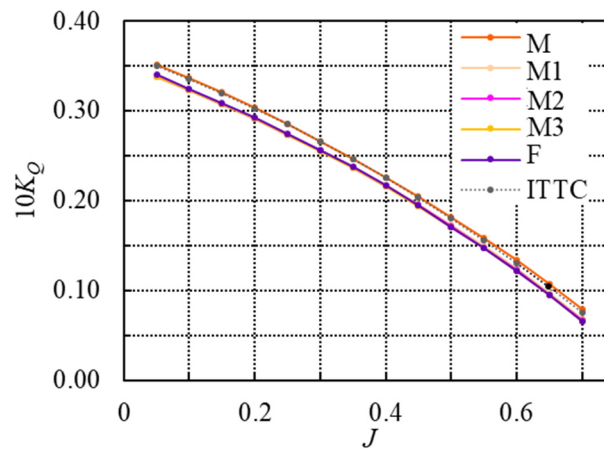


Figure 10. Torque coefficient as a function of advance coefficients for different scales.

Additionally, it is worth noting that the results of model scale numerical simulations have the same non-dimensional wall distance $y^+ > 30$ without the transition model. Large differences can be seen between the results obtained from the model scale simulations and the remaining simulations. This may be attributed to the fact that the scales for model and M1 are significantly different, i.e., $\lambda_M/\lambda_{M1} \approx 10$, and between the other scales the difference is significantly lower.

Table 7 presents the differences between the numerical values obtained for all scales at several advanced coefficients as well as the average values. These differences are calculated using the equation:

$$\Delta\phi = \frac{\phi_x - \phi_M}{\phi_M} \cdot 100\% \tag{23}$$

where ϕ stands for either K_T , K_Q , or η_o , index x denotes either M1, M2, M3, or F, and index M stands for model scale.

Table 7. The change in open water characteristics between the model scale and other scales.

<i>J</i>	M1			M2		
	$K_T, \%$	$10K_Q, \%$	$\eta_o, \%$	$K_T, \%$	$10K_Q, \%$	$\eta_o, \%$
0.1	4.37	−3.84	8.54	5.35	−4.03	9.77
0.2	4.70	−3.76	8.79	5.72	−4.09	10.22
0.3	5.61	−3.71	9.69	6.76	−4.08	11.30
0.4	7.23	−3.94	11.63	8.68	−4.40	13.68
0.5	10.12	−4.80	15.67	11.80	−5.71	18.57
0.6	17.76	−6.85	26.41	20.49	−8.24	31.31
Average	8.30	4.48	13.46	9.80	5.09	15.81

<i>J</i>	M3			F		
	$K_T, \%$	$10K_Q, \%$	$\eta_o, \%$	$K_T, \%$	$10K_Q, \%$	$\eta_o, \%$
0.1	5.79	−3.95	10.14	6.62	−3.42	10.39
0.2	5.94	−4.04	10.40	7.12	−3.59	11.10
0.3	6.81	−4.13	11.41	8.39	−3.68	12.53
0.4	8.68	−4.53	13.84	10.62	−4.18	15.45
0.5	11.83	−6.16	19.17	14.09	−5.95	21.30
0.6	21.65	−8.87	33.49	24.46	−8.74	36.38
Average	10.12	5.28	16.41	11.88	4.92	17.86

The highest average change in open water efficiencies is obtained for full-scale and it is equal to 17.86%.

Figures 11 and 12 show the obtained distribution of the skin friction coefficient at the advance coefficient $J = 0.7$ on the pressure and suction side of the propeller. The coefficient is calculated using the same density of the fluid, but with different speeds of advance for each case. It is visible that with the decrease in the scale of the propeller, the skin friction coefficient decreases, which is expected since the Reynolds number increases with the decrease in scale. The values of skin friction coefficient near the propeller hub are low with the tendency to increase at higher radii. This can be attributed to the fact that the friction velocity at higher radii is significantly higher. It is worth mentioning that the differences in skin friction coefficients for M3 and F are insignificant.

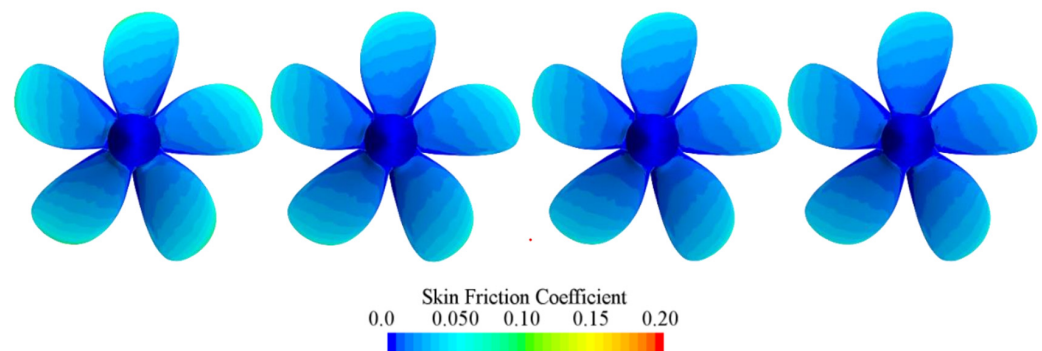


Figure 11. Distribution of the skin friction coefficient obtained from the numerical simulations at different scales on the suction side ($J = 0.7$)—M1 (first), M2 (second), M3 (third), F (fourth).

The distributions of the turbulent viscosity ratio (TVR) at $0.75R$ are presented in Figure 13. TVR is defined as the ratio between turbulent viscosity μ_t and dynamic viscosity μ . It is shown that the turbulent viscosity for the model scale is equal to zero, which suggests that the flow is laminar. For other scales, TVR around the blade profile increases with the decrease in scale. It is shown that the flow around the blade is turbulent and that the Reynolds stress increases with the decrease in scale in comparison to viscous shear stress.

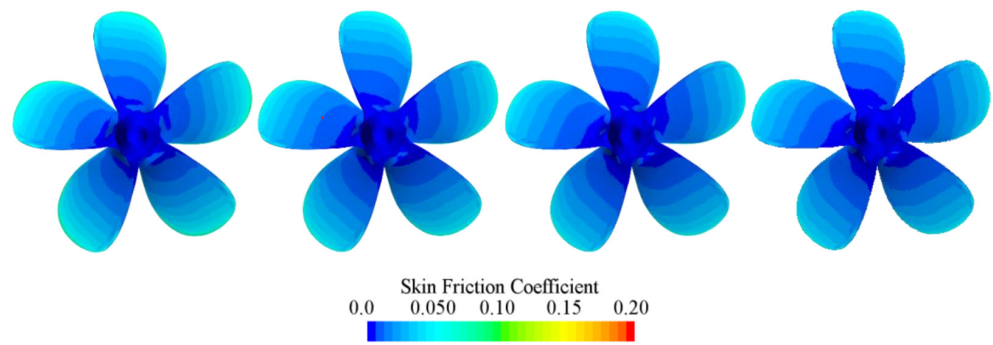


Figure 12. Distribution of the skin friction coefficient obtained from the numerical simulations at different scales on the pressure side ($J = 0.7$)—M1 (first), M2 (second), M3 (third), F (fourth).

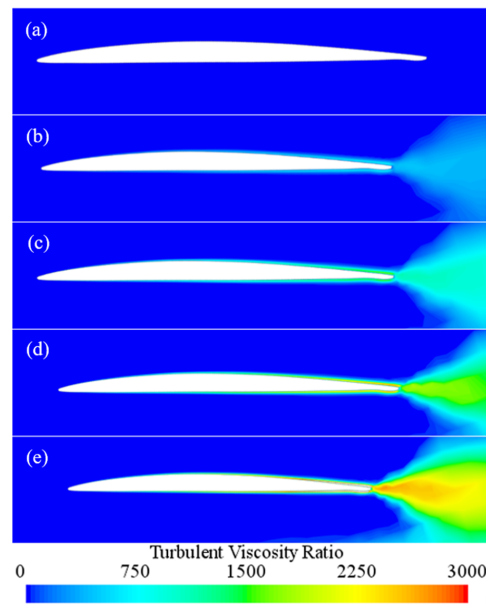


Figure 13. Turbulent viscosity ratio at $0.75R$ for $J = 0.7$ at different scales—M (a), M1 (b), M2 (c), M3 (d), F (e).

Figure 14 shows the open water efficiency for M1, M2, M3, and F propellers as well as for the model scale obtained with the transition model. It can be seen that the open water efficiency increases once the transition model is applied. From this figure, it can be seen that the impact of the scale effect on open water efficiency is significantly lower if the transition model is applied for the model scale simulations.

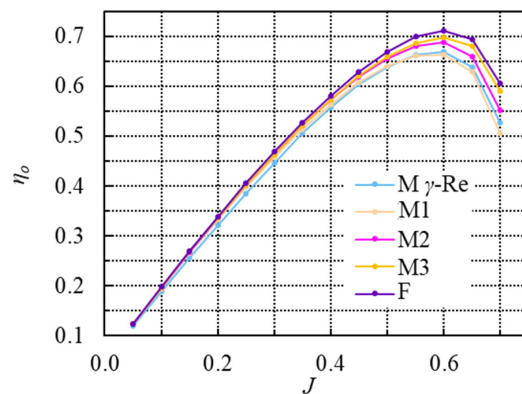


Figure 14. The obtained open water efficiencies.

4. Conclusions

Numerical simulations of the open water test (OWT) are performed at different scales. The simulation setup is described in detail as well as the meshing process. The numerical simulations of the flow around the propeller are carried out using the steady-state moving reference frame (MRF) method. Special attention is given to the grid refinements around the MRF zone and the area around the propeller to predict the flow more accurately. The shear stress transport $k - \omega$ (SSTKO) turbulence model is used to close the system of equations since it can be coupled with the Gamma Reynolds Theta ($\gamma - Re_\theta$) transition model and it is the best compromise between the accuracy and the required computational time. The non-dimensional wall distance y^+ is kept below 1 for the numerical simulations at the model scale, including the transition model, to obtain more accurate results since the laminar flow is present. Within the numerical simulations for other scales, the non-dimensional wall distance is above 30 and the transition model is disabled. The verification study is performed for spatial discretization using the grid convergence index (GCI) method, which shows that the medium size grid is appropriate in terms of computational time and the accuracy of the results. The open water curves are presented for the numerical simulations at the model scale with the transition model, which is compared to the case without the transition model. The results show that when the transition model is applied, the torque coefficient decreases, and thus the open water efficiency increases, which is also confirmed by the distribution of the skin friction coefficient. The scale effects can be noticed from the obtained open water curves, the distribution of the skin friction, as well as the turbulence viscosity ratio (TVR) field. It can be concluded that the open water efficiency increases with the decrease in scale. Finally, a comparison between the numerical simulations at the model scale with the transition model with the numerical simulations at other scales is given. It should be noted that when the transition model is applied, the scale effects on open water characteristics are significantly lower.

Author Contributions: Conceptualization, C.G.G., N.D., A.F. and I.M.; methodology, N.D., A.F. and I.M.; software, C.G.G.; validation, C.G.G.; formal analysis, C.G.G., N.D., A.F. and I.M.; investigation, C.G.G., N.D., A.F. and I.M.; resources, C.G.G., N.D., A.F. and I.M.; writing—original draft preparation, C.G.G., N.D., A.F. and I.M.; writing—review and editing, C.G.G., N.D., A.F. and I.M.; visualization, C.G.G.; supervision, N.D. and A.F.; All authors have read and agreed to the published version of the manuscript.

Funding: This study has been fully supported by the Croatian Science Foundation under project IP-2020-02-8568.

Institutional Review Board Statement: Not applicable.

Informed Consent Statement: Not applicable.

Data Availability Statement: Not applicable.

Acknowledgments: This study has been fully supported by the Croatian Science Foundation under project IP-2020-02-8568.

Conflicts of Interest: The authors declare no conflict of interest.

References

1. Farkas, A.; Degiuli, N.; Martić, I.; Dejhalla, R. Numerical and experimental assessment of nominal wake for a bulk carrier. *J. Mar. Sci. Technol.* **2019**, *24*, 1092–1104. [[CrossRef](#)]
2. Jang, Y.H.; Eom, M.J.; Paik, K.J. A Numerical Study on the Open Water Performance of a Propeller with Sinusoidal Pitch Motion. *Brodogradnja* **2020**, *71*, 71–83. [[CrossRef](#)]
3. Sun, Y.; Wu, T.; Su, Y.; Peng, H. Numerical Prediction on Vibration and Noise Reduction Effects of Propeller Boss Cap Fins on a Propulsion System. *Brodogradnja* **2020**, *71*, 1–18. [[CrossRef](#)]
4. Helma, S.; Streckwall, H.; Richter, J. The Effect of Propeller Scaling Methodology on the Performance Prediction. *J. Mar. Sci. Eng.* **2018**, *6*, 60. [[CrossRef](#)]
5. Helma, S. A scaling procedure for modern propeller designs. *Ocean Eng.* **2016**, *106*, 120, 165–174. [[CrossRef](#)]

6. Bekhit, A.S.; Lungu, A. Simulation of the POW performance of the JBC propeller. In Proceedings of the AIP Conference Proceedings, Rhodes, Greece, 13–18 September 2019.
7. Niklas, K.; Pruszek, H. Full-scale CFD simulations for the determination of ship resistance as a rational, alternative method to towing tank experiments. *Ocean Eng.* **2019**, *190*, 106435. [[CrossRef](#)]
8. Mikkelsen, H.; Walther, J.H. Effect of roughness in full-scale validation of a CFD model of self-propelled ships. *Appl. Ocean Res.* **2020**, *99*, 102162. [[CrossRef](#)]
9. Bulten, N.; Stoltenkamp, P. Full scale CFD: The end of the Froude-Reynolds battle. In Proceedings of the Fifth International Symposium on Marine Propulsion, Espoo, Finland, 12–15 June 2017.
10. Li, D.Q.; Lindell, P.; Werner, S. Transitional flow on model propellers and their influence on relative rotative efficiency. *J. Mar. Sci. Eng.* **2019**, *7*, 427. [[CrossRef](#)]
11. Brown, M.; Schroeder, S.; Balaras, E. Vortex structure characterization of tip-loaded propellers. In Proceedings of the 4th International Symposium on Marine Propulsors (SMP'15), Austin, TX, USA, 31 May–4 June 2015.
12. Dong, X.Q.; Li, W.; Yang, C.J.; Noblesse, F. RANSE-based simulation and analysis of scale effects on open-water performance of the PPTC-II benchmark propeller. *JOES* **2018**, *3*, 186–204. [[CrossRef](#)]
13. Kim, S.; Kinna, S.A. Prediction of cavitating performance of a tip loaded propeller and its induced hull pressures. *Ocean Eng.* **2021**, *229*, 108961. [[CrossRef](#)]
14. Chen, X.; Huang, Y.; Wei, P.; Zhang, Z.; Jin, F. Numerical analysis of scale effect on propeller E1619. In Proceedings of the International Conference on Offshore Mechanics and Arctic Engineering—OMAE, Madrid, Spain, 17–22 June 2018.
15. Owen, D.; Demirel, Y.K.; Oguz, E.; Tezdogan, T.; Incecik, A. Investigating the effect of biofouling on propeller characteristics using CFD. *Ocean Eng.* **2018**, *159*, 505–516. [[CrossRef](#)]
16. Tran Ngoc, T.; Luu, D.D.; Nguyen, T.H.H.; Nguyen, T.T.Q.; Nguyen, M.V. Numerical Prediction of Propeller-Hull Interaction Characteristics Using RANS Method. *Pol. Marit. Res.* **2019**, *26*, 163–172. [[CrossRef](#)]
17. Vlašić, D.; Degiuli, N.; Farkas, A.; Martić, I. The preliminary design of a screw propeller by means of computational fluid dynamics. *Brodogradnja* **2018**, *69*, 129–147. [[CrossRef](#)]
18. Mikkelsen, H.; Steffensen, M.; Ciortan, C.; Walther, J. Ship Scale Validation of CFD Model of Self-propelled Ship. In Proceedings of the MARINE 2019: Computational Methods in Marine Engineering VIII, Göteborg, Sweden, 13–15 May 2019.
19. Mejia, O.D.L.; Mejia, O.E.; Escorcía, K.M.; Suarez, F.; Laín, S. Comparison of Sliding and Overset Mesh Techniques in the Simulation of a Vertical Axis Turbine for Hydrokinetic Applications. *Processes* **2021**, *9*, 1933. [[CrossRef](#)]
20. Wang, J.; Zhao, W.; Wan, D. Simulations of Self-Propelled Fully Appended Ship Model at Different Speeds. *Int. J. Comput. Methods* **2019**, *16*, 1840015. [[CrossRef](#)]
21. A Workshop on CFD in Ship Hydrodynamics. Available online: <https://www.t2015.nmri.go.jp/> (accessed on 19 July 2022).
22. Bekhit, A.S.; Lungu, A. Numerical Study of the Resistance, Free-surface and Self-propulsion Prediction of the KVLCC2 Ship Model. In Proceedings of the International Conference on Traffic and Transport Engineering (ICTTE), Belgrade, Serbia, 27–28 September 2018.
23. Lungu, A. Numerical Simulation of the Resistance and Self-Propulsion Model Tests. *J. Offshore Mech. Arct. Eng.* **2020**, *142*, 021905. [[CrossRef](#)]
24. Farkas, A.; Degiuli, N.; Martić, I. The impact of biofouling on the propeller performance. *Ocean Eng.* **2021**, *219*, 108376. [[CrossRef](#)]
25. Farkas, A.; Degiuli, N.; Martić, I.; Dejhalla, R. Impact of hard fouling on the ship performance of different ship forms. *J. Mar. Sci. Eng.* **2020**, *8*, 748. [[CrossRef](#)]
26. Farkas, A.; Song, S.; Degiuli, N.; Martić, I.; Demirel, Y.K. Impact of biofilm on the ship propulsion characteristics and the speed reduction. *Ocean Eng.* **2020**, *199*, 107033. [[CrossRef](#)]
27. Dogrul, A. Numerical Prediction of Scale Effects on the Propulsion Performance of Joubert BB2 Submarine. *Brodogradnja* **2022**, *73*, 17–42.
28. Gonzalez-Adalid, J.; Perez-Sobrino, M.; Gaggero, S.; Gennaro, G.; Moran Guerrero, A. The use of modern computational tools in the design process of unconventional propellers for performance prediction and full-scale extrapolation. In Proceedings of the 19th International Conference on Ship and Maritime Research—NAV 2018, Trieste, Italy, 20–22 June 2018.
29. Baltazar, J.; Rijpkema, D.; Falcão de Campos, J. On the use of the Γ - $Re\theta$ transition model for the prediction of the propeller performance at model-scale. *Ocean Eng.* **2018**, *170*, 6–19. [[CrossRef](#)]
30. Moran-Guerrero, A.; Gonzalez-Gutierrez, L.M.; Oliva-Remola, A.; Diaz-Ojeda, H.R. On the influence of transition modeling and crossflow effects on open water propeller simulations. *Ocean Eng.* **2018**, *156*, 101–119. [[CrossRef](#)]
31. Pawar, S.; Brizzolara, S. Relevance of transition turbulent model for hydrodynamic characteristics of low Reynolds number propeller. *Appl. Ocean Res.* **2019**, *87*, 165–178. [[CrossRef](#)]
32. Baek, D.G.; Yoon, H.S.; Jung, J.H.; Kim, K.S.; Paik, B.G. Effects of the advance ratio on the evolution of a propeller wake. *Comput. Fluids* **2015**, *118*, 32–43. [[CrossRef](#)]
33. Farkas, A.; Degiuli, N.; Martić, I. Assessment of hydrodynamic characteristics of a full-scale ship at different draughts. *Ocean Eng.* **2018**, *156*, 135–152. [[CrossRef](#)]
34. Menter, F.R.; Langtry, R.B.; Likki, S.R.; Suzen, Y.B.; Huang, P.G.; Völker, S. A correlation-based transition model using local variables—Part I: Model formulation. *J. Turbomach.* **2006**, *128*, 413–422. [[CrossRef](#)]

35. Yao, H.; Zhang, H. Numerical simulation of boundary-layer transition flow of a model propeller and the full-scale propeller for studying scale effects. *J. Mar. Sci. Technol.* **2018**, *23*, 1004–1018. [[CrossRef](#)]
36. Bhattacharyya, A.; Krasilnikov, V.; Steen, S. A CFD-based scaling approach for ducted propellers. *Ocean Eng.* **2016**, *123*, 116–130. [[CrossRef](#)]